Available online at www.sciencedirect.com
ScienceDirect
International Journal of Multiphase Flow 33 (2007) 1237–1254
International Journal of Multiphase Flow
www.elsevier.com/locate/ijmulflow

Buffeting lift forces and local air–water flow aspects around a rigid cylinder

S. Pascal-Ribot *, Y. Blanchet

Commissariat à l'Energie Atomique DEN/DER/SSTH/LMDL, Bât. 238, CEA/Cadarache, 13108 Saint Paul Lez Durance, Cedex, France

Received 28 September 2006; received in revised form 25 May 2007

Abstract

A new experimental programme is conducted in order to relate the characteristics of two-phase flow around a rigid cylinder with the resulting lift forces. The local characteristics of air–water flow measured in the vicinity of the cylinder provide a useful source of information about the effects of flow on the excitation mechanisms. In particular, a selection of relevant parameters has been identified which, with the help of a standard dimensional analysis, may explain the energetic contents of buffeting forces. Among the parameters effective in reducing the data are the flow regime, bubble frequency and gravity forces. In addition, in the range of bubbly regimes, the magnitude of the random forces is found to be related to the local fluctuations of void fraction. Finally, a new formulation is proposed to collapse the dimensionless spectra of the buffeting lift forces in a single characteristic curve. This analysis shows a marked improvement over the collapse of data in comparison with previous normalized models.

Keywords: Two-phase flow; Buffeting lift forces; Dimensionless spectra

1. Introduction

For designing steam generators against flow-induced vibration, a reasonable assessment of tube response to the random excitation by the cross-flow is required. Resulting tube vibrations will not, usually, lead to failures on a short term basis. However, they can produce progressive damage at the supports through fretting wear or fatigue, which is a real matter of concern to the operator who aims to extend the lifetime of a nuclear plant. In PWR steam generators, tube bundles are subjected to such random excitation and the most critical zone is the U-bend region where high void fraction two-phase flow interacts transversally with the tubes.

In an attempt to assess random excitations, entirely controlled by the fluctuations inherent to the flow, the governing physical parameters have to be identified. For single-phase flow, adequate data reduction procedures (Axisa et al., 1990; Blevins, 1991) have shown that these forces are related to the turbulence level which is characterized by the dynamic pressure term. On the other hand, as underlined by Pettigrew et al. (1994), de

* Corresponding author. Tel.: +33 442 25 22 24; fax: +33 442 25 42 52.
E-mail address: spascal@cea.fr (S. Pascal-Ribot).

0301-9322/$ - see front matter © 2007 Elsevier Ltd. All rights reserved.
doi:10.1016/j.ijmultiphaseflow.2007.05.007

Langre and Villard (1998), this dynamic pressure term is no more relevant in two-phase flow. The near-field pressure fluctuations are attributed to the natural turbulence strengthened by the presence of gas or vapor bubbles. Characterization of the two-phase turbulence is still a matter of discussion, given that it is impeded by two additional difficulties, the dynamic contribution of each phase and the interfacial transfers (Nakamura et al., 1991). The random forces induced by two-phase flow have then a distinct physical origin from the single-phase flow and the physical parameters which control the magnitude of two-phase buffeting forces are still debated. For instance, assuming homogeneous flow, two different teams, Taylor et al. (1996), de Langre and Villard (1998), have developed design guidelines for two-phase turbulent buffeting forces. But, while Taylor found a significant regime effect, de Langre did not consider the flow regime effect as relevant, although the explored void fractions range from 10% to 95%. Moreover, for these latter authors, neither viscosity nor surface tension are appropriate reduction parameters; and they recognize that their tentative upper bound of the dimensionless spectra of buffeting forces does not provide any explanation of the origin of fluctuating forces. More recently, Taylor and Pettigrew (2001) have shown that random excitation forces are dependent on both void fraction and flow regime. Nevertheless, since 2001, a number of specific situations have been identified in which the design margins should be reduced or, at least, more precisely evaluated. This indicates a need to improve our knowledge of the parameters involved in the mechanisms of buffeting forces.

The techniques to detect these physical parameters use input from a huge number of experimental data. In single-phase cross-flow the problem has been approached with a single tube (So and Savkar, 1981; Cheung and Melbourne, 1983) as well as with tube bundles (Axisa et al., 1990; Blevins, 1991; Endres and Moller, 2001). In two-phase cross-flow, compared with the considerable amount of work reported in the open literature about tube arrays (Taylor et al., 1989, 1992; Nakamura et al., 1991; Oengoren and Ziada, 1995; Inada et al., 2004 to name a few), the single cylinder has been insufficiently documented although it constitutes a basic analytical step to understand the underlying physics. The only information available in this area seem to refer to vortex sheddings (Hara, 1982; Inoue et al., 1986) and bubble tracking (Murai et al., 2005) rather than buffeting forces. A new experimental programme is proposed here to progress in this situation. This programme describes experiments with an horizontal cylinder across an air–water flow and aims at relating the flow characteristics with the resulting lift forces. The present paper discusses the first stage of this programme, where the local flow parameters are characterized with a bi-optical probe, and the lift forces are measured with a force cell on the cylinder. The explored void fractions range from 10% to 80%.

2. Experimental aspects

2.1. Test section

The AMOVI test channel (Fig. 1) is a long acrylic rectangular duct (0.65 m for the straight part), with a $0.07\ \text{m} \times 0.1\ \text{m}$ cross section, which contains a transverse single cylinder. The cylinder is rigid and 0.1 m long with an outer diameter $D = 12.15 \times 10^{-3}$ m. Water and air flow co-currently upwards. The mock-up is supplied with a water flow rate between 5×10^{-6} and $2 \times 10^{-3}\ \text{m}^3/\text{s}$ and an air flow rate between 2×10^{-6} and $2.2 \times 10^{-2}\ \text{m}^3/\text{s}$. It operates at atmospheric pressure and ambient temperature. The correct mixture of both phases is ensured by a specific mixer (Fig. 2).

2.2. Instrumentation

For the measurement of the local two-phase flow parameters a bi-optical probe intrusive technique is used (Galaup, 1975; Delhaye et al., 1981). This technique is based on the phase density function given by each sensor response. Ideally, the sensor response is 1 inside the gas and 0 inside the liquid. Thus from the signal given by upstream and downstream sensors, this technique allows the measurement of parameters such as the bubble count rate f_b, the bubble velocity V_{mb}, the bubble chord length CL_b and one of the main two-phase geometric parameters, the void fraction α. In the present experiments, the bi-optical probe (BOP) is inserted at the centerline of the test column and positioned 0.03 m upstream from the cylinder (Figs. 1 and 3). Moreover, thanks to a micrometer screw, this BOP can move across the test section, allowing the record of the axial profiles of the previous parameters. The geometric characteristics of the BOP (Fig. 4) are:

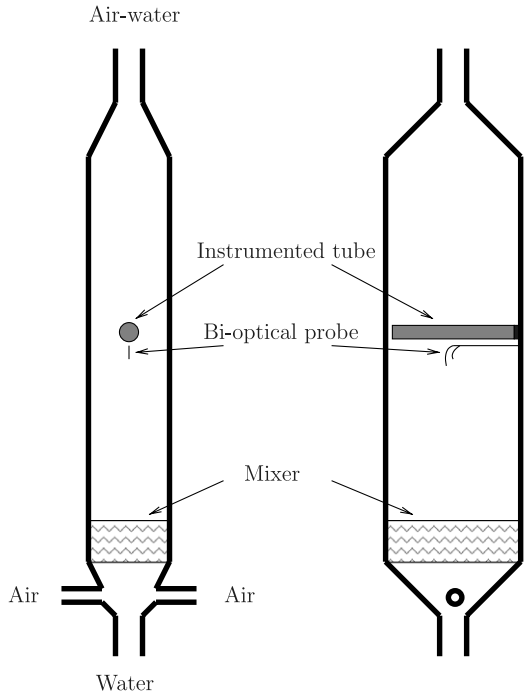

Fig. 1. Scheme of Amovi mock-up.

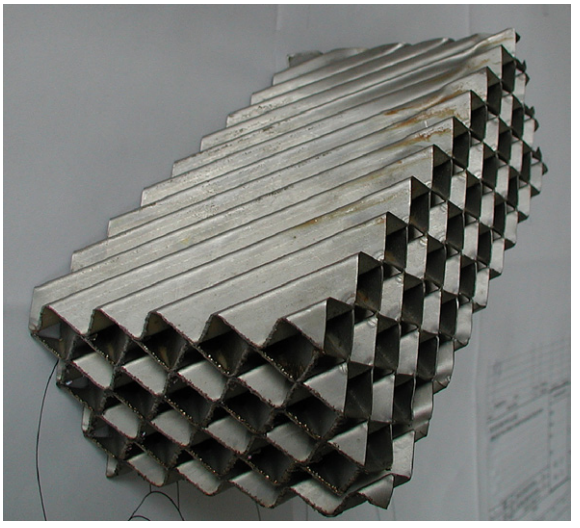

Fig. 2. Air–water mixer.

– 1.35×10^{-3} m for the distance between the upstream and downstream sensors,
– optical fiber of 2×10^{-4} m diameter with conical tips.

To measure the fluid lift force acting on the cylinder, a load cell is employed. The sensor is triaxial piezoelectric and positioned at the tube extremity. A static calibration has been performed for both drag and lift components with suspended weights. The first natural frequency of the instrumented cylinder is about 500 Hz which leads us to assume that between 0 and 250 Hz, our range of interest, the cylinder provides with a ''static'' response.

Fig. 3. Test section photograph.

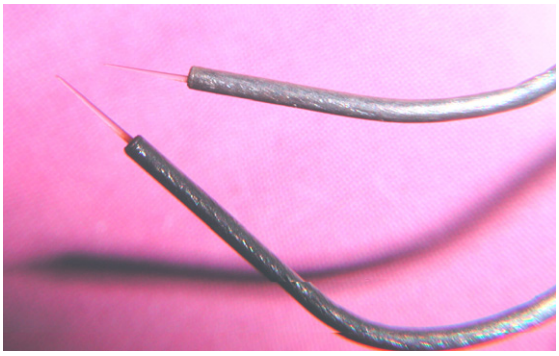

Fig. 4. Bi-optical probe photograph.

Both the liquid and air flow rates are measured by flowmeters located at the mixer inlet. The liquid and gas superficial velocities, J_l and J_g, are obtained by:

$$J_l = \frac{Q_l}{A}, \quad J_g = \frac{Q_g}{A}$$

where A is the cross section of the test channel, Q_l and Q_g stand for the volume flow rate of liquid and gas respectively.

2.3. Data processing and calculations

The sampling frequency for bi-optical probe is 200 kHz. Signals are recorded at each change in refractive index during 600 s or until 50,000 events are recorded.

The force signal is recorded with a sampling frequency of 2.5 kHz during 655 s.

(a) The local time-averaged two-phase flow parameters are calculated as follows:

- *Bubble count rate*: The total number of bubbles or events acquired by the probe upstream sensor is divided by the total acquisition time:

$$f_{\mathrm{b}} \triangleq \frac{N_{\mathrm{b}}}{T} \tag{1}$$

- *Void fraction*: The total gas residence time acquired by the probe upstream sensor is divided by the total acquisition time:

$$\alpha \triangleq \frac{\sum_{j=1}^{N_{\mathrm{b}}} (\Delta t_{\mathrm{g}})_j}{T} \tag{2}$$

- *Measured bubble velocity*: The local measured jth bubble velocity is computed from the information given by both upstream and downstream sensors:

$$(V_{\mathrm{mb}})_j \triangleq \frac{s}{(\Delta t_{\mathrm{front}})_j}$$

where s is the distance between the upstream and downstream sensors. $\Delta t_{\mathrm{front}}$ is the time lag, generated by the front interface, measured by the upstream and downstream sensors. Only the rising slopes are considered here.The local time-averaged velocity is calculated over all the acquired front interface during the total acquisition time:

$$V_{\mathrm{g}} = \frac{1}{N_{\mathrm{b}}} \sum_{j=1}^{N_{\mathrm{b}}} (V_{\mathrm{mb}})_j = \frac{s}{N_{\mathrm{b}}} \sum_{j=1}^{N_{\mathrm{b}}} \left(\frac{1}{\Delta t_{\mathrm{front}}} \right)_j \tag{3}$$

- *Bubble chord length*: The chord length corresponds to the actual distance traverse by the sensor inside a bubble. It is calculated from the jth bubble residence time and the measured bubble velocity:

$$(\mathrm{CL_b})_j = (V_{\mathrm{mb}})_j (\Delta t_{\mathrm{g}})_j \tag{4}$$

The Sauter mean diameter, d_{b}, is chosen to characterize the bubble size. It corresponds to an average diameter on "credible" bubble diameters deduced from a bubble chord length analysis.

(b) The load cell provides with a direct measurement of the flow-induced forces integration on the tube length L_T (Axisa et al., 1990; Nakamura et al., 1991). So that the force transducer spectral response, Φ_R, is defined from flow-induced forces autocorrelation spectrum:

$$\Phi_R(s,f) = \int_0^{L_T} \int_0^{L_T} H(s,s_1,f) H^*(s,s_2,f) \Psi_F(s_1,s_2,f)\, \mathrm{d}s_1\, \mathrm{d}s_2 \tag{5}$$

where $H(s,s_1,f)$ characterizes the transfer function of the tube between s and s_1. H^* denotes the complex conjugate of H.

Following Axisa et al. (1990), Ψ_F is defined separating the dependence on space variables (s_1,s_2) and frequency (f). The space dependence is now characterized through a correlation length λ_{c} as

$$\Psi_F(s_1,s_2,f) = \Phi_F(f) \mathrm{e}^{-\frac{|s_1 - s_2|}{\lambda_{\mathrm{c}}}} \tag{6}$$

where $\Phi_F(f)$ is the autocorrelation spectrum of the turbulent forces per unit tube length. Using the scaling factors, P_0 and f_0 defined in Section 4, this local spectrum is reduced to a dimensionless form:

$$\overline{\Phi_F\left(\frac{f}{f_0}\right)} = \frac{\Phi_F(f)}{\frac{(P_0 D)^2}{f_0}} \tag{7}$$

Then, assuming that $\frac{\lambda_c}{L_T}$ is small, Eq. (5) can be written

$$\Phi_R(s,f) = 2 * L_T \int_0^{L_T} H(s,s_1,f)^2 \Phi_E(f)\,\mathrm{d}s_1 \tag{8}$$

where Φ_E, the equivalent spectrum of the turbulent forces can be assimilated with the fully correlated random forces per unit length. These latter would have the same effect on the cylinder as the forces defined in Eq. (6). The dimensionless form of Φ_E, introduced by Axisa et al. (1990), is defined as

$$\overline{\Phi_E\left(\frac{f}{f_0}\right)} = \frac{\lambda_c}{L_T}\overline{\Phi_F\left(\frac{f}{f_0}\right)} \tag{9}$$

Practically, the adaptation from one geometrical configuration to another is performed using the dimensionless reference equivalent spectrum, $\overline{\Phi_E^0}$, defined by

$$\overline{\Phi_E^0\left(\frac{f}{f_0}\right)} = \left(\frac{L_T}{L_0}\right)\left(\frac{D_0}{D}\right)\overline{\Phi_E\left(\frac{f}{f_0}\right)} \tag{10}$$

where L_0 and D_0 are reference lengths. As de Langre et al. (1991), Axisa and Villard (1992), the present work supposes $L_0 = 1$ m and $D_0 = 0.02$ m.

2.4. Test matrix

The experimental dataset subject of this investigation is composed of 16 tests ranging in the domain of local void fractions $10\% \leqslant \alpha \leqslant 80\%$; the test matrix was initially determined from the homogeneous void fraction, $\alpha_H = \frac{Q_g}{Q_g + Q_l}$, which ranges from 30% to 95% ($\alpha_H = 30\%$, 50%, 80%, 90%, 95%). Not surprisingly, the homogeneous void fraction does not coincide with the local value. The drawback of this methodology results in the irregular distribution of the measured void fraction values within the domain investigated. In particular the range $20\% \leqslant \alpha \leqslant 40\%$ will not be represented.

Table 1 gives the test operating conditions as well as the associated response of each optical fiber (subscripts 1 and 2). The signal correlation of both fibers results in the values of V_g and d_b collected in Table 2.

Table 1
New experimental AMOVI database

Test no.	$Q_{water} \times 10^3$ (m^3/s)	$Q_{air} \times 10^3$ (m^3/s)	T_{acq} (s)	α_1	α_2	N_{b_1}	N_{b_2}	f_{b_1} (Hz)	f_{b_2} (Hz)
19	1.00	1.00	599.65	0.20	0.19	19,459	18,323	32.45	30.56
20	0.20	0.20	599.65	0.14	0.14	14,269	13,639	23.80	22.75
21	1.50	1.50	599.65	0.17	0.15	16,202	14,485	27.03	24.16
22	1.64	0.70	599.65	0.11	0.10	10,654	9561	17.80	15.95
23	1.00	0.40	599.65	0.12	0.11	10,499	9542	17.50	15.92
24	0.47	0.20	599.65	0.13	0.12	13,358	13,026	22.28	21.73
25	0.05	0.20	599.65	0.13	0.12	11,576	11,297	19.30	18.84
26	0.50	2.00	586.06	0.44	0.45	49,998	49,834	85.31	85.04
27	1.00	4.50	599.65	0.41	0.42	45,000	45,154	75.04	75.30
28	0.80	9.72	364.39	0.62	0.63	49,999	49,931	137.22	137.03
29	0.40	7.60	391.51	0.68	0.69	49,999	49,258	127.71	125.82
30	0.25	4.75	446.96	0.65	0.66	49,999	49,494	111.87	110.74
31	0.40	9.72	370.78	0.72	0.72	49,998	49,319	134.85	133.02
32	0.25	9.72	364.21	0.74	0.74	49,999	49,470	137.28	135.83
36	1.02	9.17	350	0.52	0.52	50,000	50,000	142.86	142.86
37	0.65	22.22	350	0.80	0.80	50,000	50,000	142.86	142.86

Table 2
New experimental AMOVI database (continued)

Test no.	V_g (m/s)	d_{b_1} (mm)	d_{b_2} (mm)
19	0.52	4.8	4.8
20	0.63	5.7	5.7
21	0.40	3.7	3.7
22	0.32	3.0	3.0
23	0.39	3.9	3.9
24	0.53	4.5	4.6
25	0.65	6.4	6.5
26	1.11	8.7	8.8
27	1.01	8.4	8.5
28	1.46	9.9	10.1
29	1.63	13.0	13.3
30	1.54	13.5	13.7
31	1.71	13.7	13.9
32	1.81	14.6	14.9
36	1.20	8.3	8.4
37	2.16	13.8	13.9

3. Measurements analysis

3.1. Two-phase flow analysis

In a first step, it is proposed to gain indications on the flow characteristics by way of some graphic observations. In these experiments, five parameters, α, V_g, V_l, f_b and d_b are of central concern. The resulting choices do not pretend to completely explain the mechanisms of excitation observed in this mock-up but they are supported by the fair collapse of data gained onto a characteristic dimensionless representation.

3.1.1. Flow regimes

The different geometrical configurations of two-phase flows, or flow regimes, depend on the fluid properties, the size of the channel and the flow rate of each phase. For fixed fluid properties and channel, the flow regime is entirely determined by Q_g and Q_l, the gas and liquid flow rates.

On the basis of theoretical considerations, Taitel et al. (1980) have developed a reference map for predicting flow regime transitions in vertical tubes. For a given value of $J_l = 0.4$ m/s for instance, these authors consider a continuous transition between bubble, slug, slug or churn, and annular regimes for vertical tubes 0.05 m diameter. A representation of the AMOVI test conditions on this map would indicate that the tests are mainly concerned with bubbly and slug flow regimes, the churn flow regime affecting only one test at 80% void fraction.

However, studying the bubble-slug transition in a 0.150 m diameter cylindrical column, Cheng et al. (1998) report that traditional slug flow does not exist in such a column and is replaced by a gradual transition to churn flow. Possible instabilities of void fraction waves are detected during the transition from bubble to churn at constant liquid rate. The fact that the churn flow is dominant in a large vertical pipe ($D = 0.2$ m) under the conditions where small-scale pipes have slug flow has already been mentioned in Mishima and Ishii (1984).

With a 0.07×0.10 m cross section, the rectangular duct used in AMOVI tests is likely to present an intermediate situation between those small-scale and large diameter cylindrical pipes. In addition, the relatively short distance between the air–water mixer and the location of measurements does not allow for a completely developed flow. This explains why no remarkable slug frequency has been noticed during the tests, neither visually nor after signal processing. These different arguments support the hypothesis of a direct bubble-churn transition in the present data as indicated in Fig. 5 which separates bubbly flow regimes under 20% void fraction from churn-turbulent flow regimes beyond 20%.

This partial flow regime map depicts a global and rather qualitative aspect, but the primary point to remember is that two distinct categories of experimental data have been evidenced, relative to bubbly and

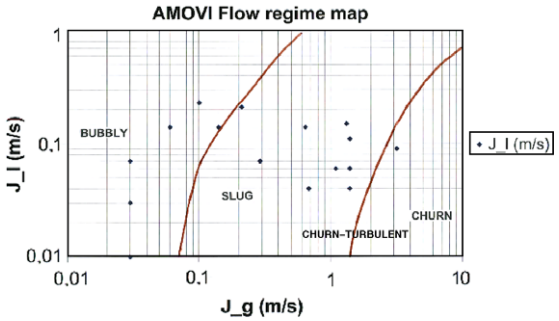

Fig. 5. Flow regime map.

churn-turbulent flow regimes. Since the flow regime is a way in which phases distribution lead to differences in physical behaviour, it remains to be seen whether this flow characteristic is related to the level of energy in the forces spectra. By providing a more local and quantitative information, some basic observations on the measurements by BOP will help supporting this assumption.

3.1.2. Local flow parameters

This section discusses the evaluation and trends of the most important local flow parameters, namely the void fraction, liquid and gas velocities, Sauter mean diameter and bubble count rate. Among these parameters, V_g characterizes the two-phase dynamics, α and d_b are more specific of the granular structure of the two-phase flow, and f_b belongs to both categories.

(1) *Void fraction*: For the whole values of α, Fig. 6 compares the local void fraction to the values estimated by the drift flux model of Zuber–Findlay as well as the homogeneous model and the model of Ishii. It can be seen that the averaged Zuber–Findlay model generally agrees with the local measurements, except for a few tests where the void fraction is significantly overestimated. In contrast, the Ishii model underestimates the local void fraction. The homogeneous model not only greatly overestimates the local value, but is not sensitive enough to flow rate changes. Moving on now to axial profiles of void fraction the results of some measurements are illustrated by Fig. 7. In dedicated runs, the BOP was repositioned every 10^{-2} m in the cross direction for three different values of α. These profiles obtained in a rectangular channel are consistent with those reported by Serizawa et al. (1997), Grossetête (1995) for a circular channel. They are rather flat for mean void fraction ranging from 10% to 20% and become parabolic

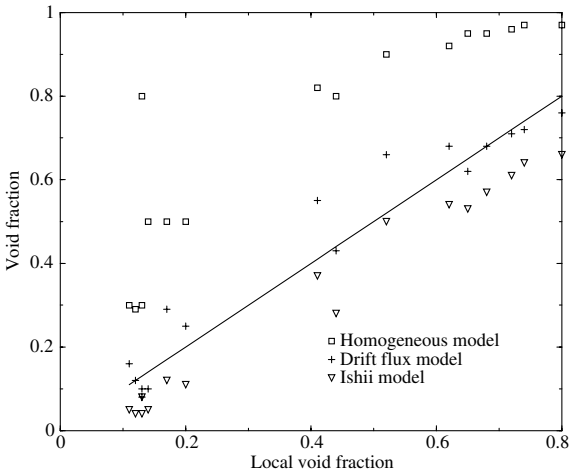

Fig. 6. Void fraction models versus the measured local void fraction.

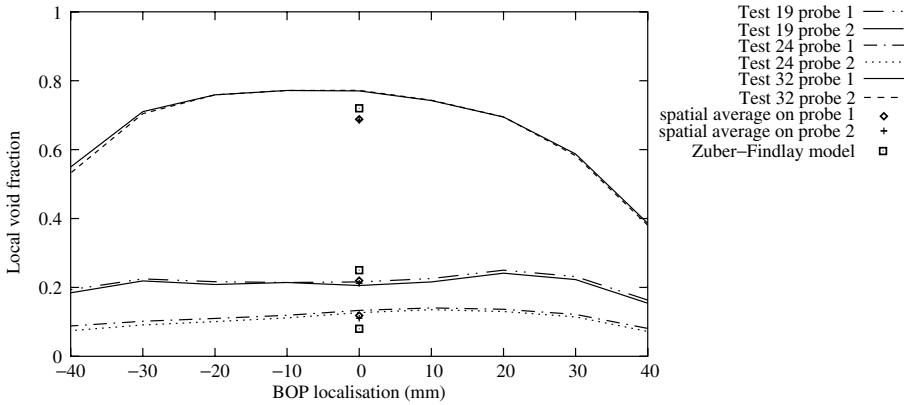

Fig. 7. Profile of the local void fraction in the test section.

as the mean void fraction increases. Calculations of the mean void fraction by two different ways, the Zuber–Findlay drift flux model and a spatially-averaged mean of the measured values, are reported on the same figure. It is seen that both fibers give similar mean values of the void fraction, which are very close to the local value for $\alpha \leqslant 20\%$. The drift flux model overpredicts the spatially-averaged mean void fraction for $\alpha \geqslant 20\%$.

In general when the local void fraction values are not available, the Zuber–Findlay drift flux model appears to be the most representative of the gas presence.

(2) *Liquid velocity*: In the absence of measurements, this parameter was estimated as

$$V_1 = \frac{Q_1}{(1-\alpha)A} = \frac{J_1}{(1-\alpha)} \tag{11}$$

which combines a local variable α with an average variable, Q_1. As a result, the experimental conditions cover 0.01–0.45 m/s for the liquid velocity, which corresponds to an interval of 0.44 m/s between the minimum and maximum.

In Fig. 8, V_1 is plotted against the local void fraction. This figure does not arise any particular comment. For that reason the variable V_1 was not found convincing at this step of the analysis.

(3) *Gas velocity*: The bubble axial velocity, V_g, measured by the BOP varies in the range 0.32–2.16 m/s that is four times greater than for the liquid velocity. The variation of V_g is represented against the local void fraction in Fig. 9.

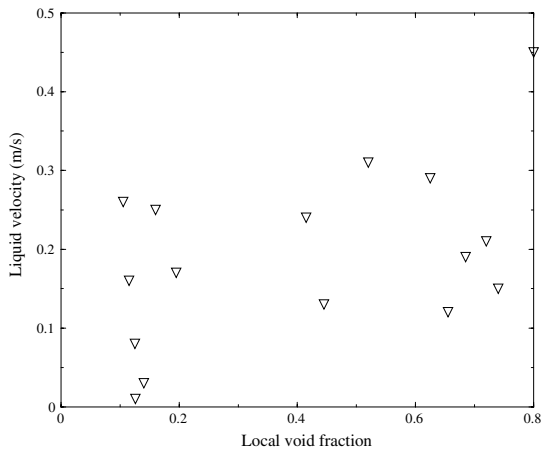

Fig. 8. Evolution of the liquid velocity versus the local void fraction.

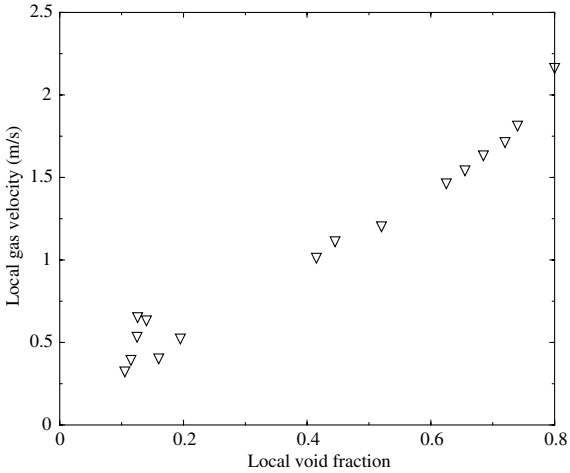

Fig. 9. Evolution of the gas velocity versus the local void fraction.

Two distinct regions are observed in this figure:

- a bell shape for $\alpha \leqslant 20\%$,
- a monotonous increasing variation from $\alpha = 20\%$.

This curve clearly indicates a possible link between the bubble axial velocity and the flow regime in the whole range of the investigated void fractions. Consequently, this variable is likely to be among variables which describe the physics of two-phase flow.

(4) *Relative velocity*: The gas velocity can also be represented using the relative velocity of bubbles determined by $V_r = V_g - V_l$. This variable varies in the range 0.06–1.71 m/s that is the same order of value as the range of V_g.
Fig. 10 displays the relation between V_r and the local void fraction. It appears that the evolution is very similar to the evolution of V_g and prompts us to consider this variable at the same level of interest as V_g.

(5) *Sauter mean diameter*: The Sauter mean bubble diameter also deserves a particular attention. It corresponds to the equivalent spherical diameter by surface area per unit volume to the full distribution. As for flow regime, d_b depends on the fluids properties, the superficial gas and liquid velocities (J_g, J_l) and the channel size. Fig. 11 plots d_b against the local void fraction. As expected, the d_b evolution cor-

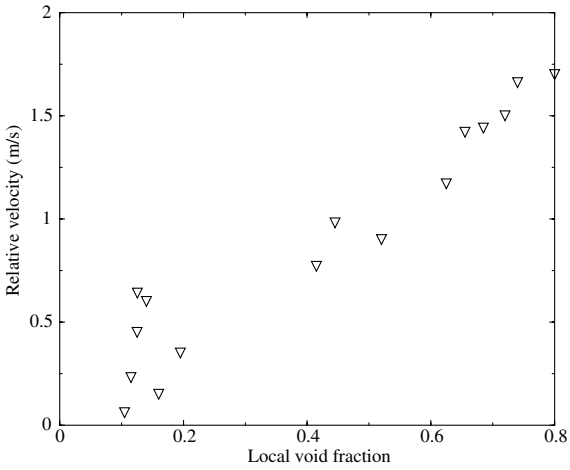

Fig. 10. Evolution of the relative velocity versus the local void fraction.

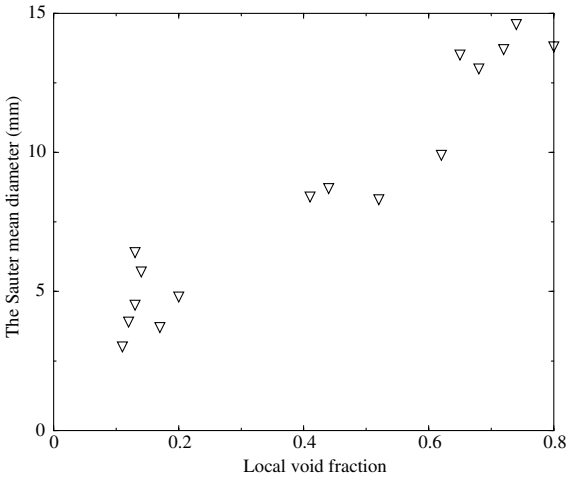

Fig. 11. Evolution of Sauter mean diameter versus the local void fraction.

responds to the V_g evolution. The two regions identified in the V_g variation are still observable. These two regions are probably in relation with the bubble shapes associated with the characteristic trajectories described in Hassan et al. (1998). The boundary between "distorted bubbles" and cup bubbles can be characterised by the Ishii and Zuber (1979) critical diameter, $d_c = 4\sqrt{\frac{\sigma}{\Delta\rho g}}$. In the present experiments, $d_c = 0.011$ m, which corresponds to the tests where $\alpha > 60\%$. As a result d_b is listed as a relevant parameter for the two-phase flow characterization.

(6) *Bubble count rate*: When considering the forces exerted on the obstacle it seems natural to pay attention to the bubble count rate measured by the BOP and which characterizes the bubble's collision frequency with the cylinder. For Murai et al. (2005) it is one of the parameters which determines the spatial scale of the single-phase wake region. Fig. 12 represents the bubble count rate, measured on the upstream probe, as a function of the local measured void fraction. Bubble count rate increases with the local void fraction until $\alpha = 20\%$. Above $\alpha = 41\%$ the slope rises dramatically before reaching a plateau around $\alpha = 50\%$. It clearly shows three different behaviours including the two aforementioned flow regimes: bubbly when $\alpha \leqslant 20\%$ and churn-turbulent beyond.

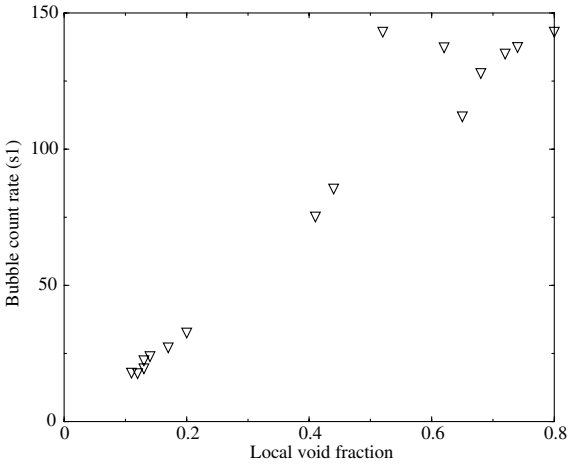

Fig. 12. Bubble count rate measured on the upstream probe.

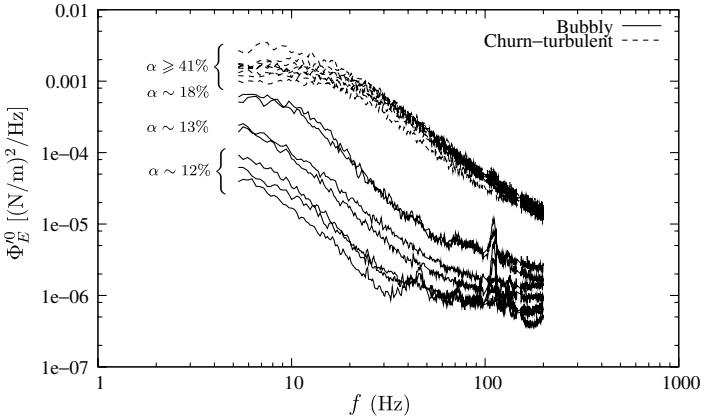

Fig. 13. Evolution of the reference equivalent spectra versus frequency.

3.2. Spectral analysis of buffeting forces

The analysis of the original spectra allows to collect general information about the effects of frequency and local void fraction on the total amount of energy. Power spectral densities Φ_E^0 issued from the 16 experiments are plotted against frequency in Fig. 13. Their observation leads to three main conclusions:

(1) As expected, the flow contains strong low frequency components which also produce significant nonresonant buffeting of the structure. After about 20 Hz, the decrease of the power spectral density is generally accelerated. Moreover, as the void fraction increases, low frequency components increase. In the same time the steep slope decreases.
(2) For $11\% \leqslant \alpha \leqslant 20\%$ the spectra exhibit a clear dependence on void fraction: the spectra amplitudes increase with void fraction.
(3) From $\alpha = 41\%$ (no observations between 20% and 41%) a different behaviour is noticed, as well of the amplitude of spectra as of the decreasing slope: all the spectra are collapsed and the value of the void fraction does not seem to have any influence.

These findings combined with the remarks of the Section 3.1.1 on flow regime confirm that, concerning two-phase buffeting forces, flow regime is a relevant parameter. As long as flow regime is bubbly, the void fraction plays a major role on the levels of the spectra. On the other hand for churn-turbulent regime, void fraction seems to have no influence.

As a result, since beyond $\alpha = 41\%$ the spectra are already clustered, most of analyses have been focussed on experiments classified in bubbly regime (Fig. 5).

3.3. Identification of additional variables

In addition to the aforementioned analysis of experimental data as well as to earlier work by the present authors (Pascal-Ribot and Blanchet, 2005), a number of supplementary variables and dimensionless numbers have been investigated. Partially mentioned as relevant by several researchers – see, for instance, Mercadier (1981) and Friberg (1998) – these variables are related to the momentum transfer, gravity, flow compressibility, inertial and friction effects. Examination of the behaviour of these variables in our experiments has revealed two important aspects:

- First, a confirmation of the weight already attributed to the parameters V_g, V_r and d_b,
- Second, in our earlier selections, the lack of attention to a significant variable, namely the void fraction fluctuations. Following the main idea developed by Le Gall et al. (2001), the void fraction fluctuations

are suspected to play a major role on flow-induced forces. According to previous remarks, this phenomenon is noticeable in bubbly regime. In contrast, for churn-turbulent regime, flow-induced forces do not seem to depend on the void fraction and consequently no longer on its fluctuations. In Matuszkiewicz et al. (1987) work performed in a free square channel, the profile of the void fraction fluctuations follows a $\alpha^2(1-\alpha)$-like law for a mean void fraction below 35% while in Lian et al. (1997) work, performed in tube bundle, this profile is closer to a $\alpha(1-\alpha)^2$ law. As a result, for our free channel, the void fraction fluctuations will be characterized by the Matuszkiewicz law, i.e $\alpha^2(1-\alpha)$ for the bubbly regime. In case of churn-turbulent regime, it is assumed that the level of the void fraction fluctuations reaches a maximum (around $\alpha_{ct} = 40\%$) before decreasing.

Finally, the following preliminary conclusions can be drawn:

- the observation of the local two-phase flow characteristics leads to the hypothesis of two flow regimes, which is of primary importance for the ensuing investigation of the force spectra,
- the parameters related to void fraction, gravity, gas velocity, bubble size and frequency influence the spectral magnitude of the lift forces on cylinder. The following variables may be considered as relevant: α or $\alpha^2(1-\alpha)$, ρ_l, ρ_g,V_g or V_r, d_b and f_b.

4. Proposal of dimensional analysis

A major point is the importance of separating competing from cooperating effects and how dimensionless groups inherently do this. To make the point, we combine, in the following, the interpretation of experiments with dimensional analysis. This section is concerned mostly with a new scaling relationship of the buffeting forces power spectral density, that will provide a significant improvement in collapse of data.

Substituting Eqs. (7), (9) into Eq. (10), the dimensionless form for the reference equivalent spectrum can be expressed by

$$\overline{\Phi_E^0\left(\frac{f}{f_0}\right)} = \frac{f_0}{(P_0 D)^2}\Phi_E'^0(f) \tag{12}$$

with $\Phi_E'^0(f) = \left(\frac{L_T}{L_0}\right)\left(\frac{D_0}{D}\right)\frac{\lambda_c}{L_T}\Phi_F(f)$. The scaling parameters P_0 and f_0 refer respectively to a pressure scale and to a time scale.

4.1. An improved model for dimensionless spectra

The search for adequate scaling parameters, P_0 and f_0, is supported by the physical parameters previously identified for their involvement in buffeting forces. Then, the following scaling parameters are proposed for the bubbly regime:

– the tube diameter, D,
– a flow characteristic length comparable to those proposed by Taylor et al. (1996) or more recently by de Langre and Villard (1998), and representative of the void fraction fluctuations (Matuszkiewicz et al., 1987), $L_f = \alpha^2(1-\alpha)\sqrt{\frac{\sigma}{\Delta\rho g}}$. In the present experiments the term $\sqrt{\frac{\sigma}{\Delta\rho g}}$, called the Laplace length, is a constant. It defines a critical length for bubbly flows and participates to the well-known Ishii and Zuber (1979) drag coefficient correlation,
– the bubble count rate, f_b,
– the force fluctuations frequency, f,
– a static lineic force, $E_s = \rho g D^2$ with $\rho = \alpha\rho_g + (1-\alpha)\rho_l$. Assuming $\alpha\rho_g \ll (1-\alpha)\rho_l$ the static lineic force is reduced to $E_s = (1-\alpha)\rho_l g D^2$.

The unknown parameter, noted F^*, defines the force resultant exerted on cylinder per unit length: $F^* = \frac{F}{L_T}$. Then the functional dependency of F^* on the previously mentioned variables is expressed by

$$F^*(D, L_\mathrm{f}, f_\mathrm{b}, f, E_\mathrm{s})$$

Application of the Π theorem leads to the three dimensionless parameters:

$$\pi_F = \frac{F^*}{E_\mathrm{s}}; \quad \pi_{L_\mathrm{f}} = \frac{L_\mathrm{f}}{D}; \quad \pi_f = \frac{f}{f_\mathrm{b}};$$

Following Szirtes (1997) to determine the force on an immersed body in single-phase viscous liquid, we assume a monomial form for F^*

$$F^* = kE_\mathrm{s}\left(\frac{L_\mathrm{f}}{D}\right)^{\epsilon_1}\left(\frac{f}{f_\mathrm{b}}\right)^{\epsilon_2}$$

where k is a constant.

In order to have the lift force scaling parameter directly proportional to the obstacle frontal area, ϵ_1 is set to 1. This leads to

$$F^* = k\rho_\mathrm{l} gD\sqrt{\frac{\sigma}{\Delta\rho g}}[\alpha(1-\alpha)]^2\left(\frac{f}{f_\mathrm{b}}\right)^{\epsilon_2}$$

Say, in pressure term,

$$P = \frac{F}{DL_T} = \frac{F^*}{D} = k\rho_\mathrm{l} g\sqrt{\frac{\sigma}{\Delta\rho g}}[\alpha(1-\alpha)]^2\left(\frac{f}{f_\mathrm{b}}\right)^{\epsilon_2}$$

where (DL_T) is the cylinder frontal area.

Scaling factors for reference equivalent force spectra can be chosen as

$$\begin{aligned} P_0 &= k\rho_\mathrm{l} g\sqrt{\frac{\sigma}{\Delta\rho g}}[\alpha(1-\alpha)]^2 \\ f_0 &= f_\mathrm{b} \end{aligned} \tag{13}$$

However, as already mentioned, the notion of bubbles is suitable only for bubbly flow regime. In churn-turbulent regime, the relative velocity, V_r, is preferred as a frequency characteristic parameter (Pascal-Ribot and Blanchet, 2005). Applying a similar development to churn-turbulent regime leads to

$$\begin{aligned} &F^*(D, L_{\mathrm{f}_\mathrm{ct}}, V_\mathrm{r}, f, E_\mathrm{s}) \\ &P_0 = k\rho_\mathrm{l} g\sqrt{\frac{\sigma}{\Delta\rho g}}[\alpha_\mathrm{ct}(1-\alpha_\mathrm{ct})]^2 \quad \text{with } \alpha_\mathrm{ct} = 0.4 \\ &f_0 = \frac{V_\mathrm{r}}{D} \end{aligned} \tag{14}$$

Remark: No value has been imposed to the exponent ϵ_2 since the scaling parameter for frequency is directly seen as f_b or $\frac{V_\mathrm{r}}{D}$ according to the flow regime. By comparison with single-phase study (Blevins, 1991), ϵ_2 is supposed equal to 1 in the churn-turbulent case, which leads to a "mixture Strouhal number", $\mathscr{S} = \frac{fD}{V_\mathrm{r}}$.

For the present applications the constant k has been set to 1 for both bubbly and churn-turbulent flow regimes. Moreover, since the experiments have been conducted with a single mixture (air–water), the term $\rho_\mathrm{l} g\sqrt{\frac{\sigma}{\Delta\rho g}}$ is a constant. Consequently, even if gravity is known to induce a difference between gas and liquid velocities which might be related to dynamic pressure, its pertinence as well as the one of surface tension cannot be assessed without additional experiments.

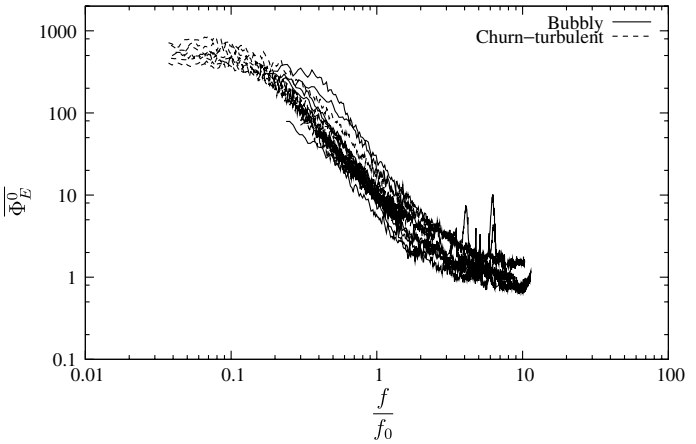

Fig. 14. Dimensionless reference equivalent spectra using Eqs. (13) and (14).

4.2. Applications on AMOVI programme

Fig. 14 shows the dimensionless spectra calculated with Eqs. (12)–(14). We observe that the proposed dimensionless parameters yield a remarkable collapse of the measured buffeting forces spectra both in terms of the reduced frequency and of the force levels. Compared with experimental results (Fig. 13), which spread over two decades, the spread of the present spectra is only half a decade.

In Fig. 15, the same spectra are scaled with the scaling parameters, P_0 and f_0, previously proposed for tube bundle by de Langre and Villard (1998), namely

$$\begin{aligned} P_0 &= \rho_l g D_w \quad \text{with } D_w = 0.1D/\sqrt{1-\alpha_H} \\ f_0 &= \frac{V_H}{D_w} \end{aligned} \tag{15}$$

where the subscript H relates to the homogeneous model.

Although Eq. (15) was mainly aimed at proposing an upper bound for experiments with various geometries and fluids, its authors have progressed by successively improving the collapse of dimensionless spectra. Apparently, applied to our present data, these scaling factors lead to different reduction effects both in terms of reduced frequency and of force levels (see Fig. 15). As a matter of fact, a part of the reduced spectra is beyond

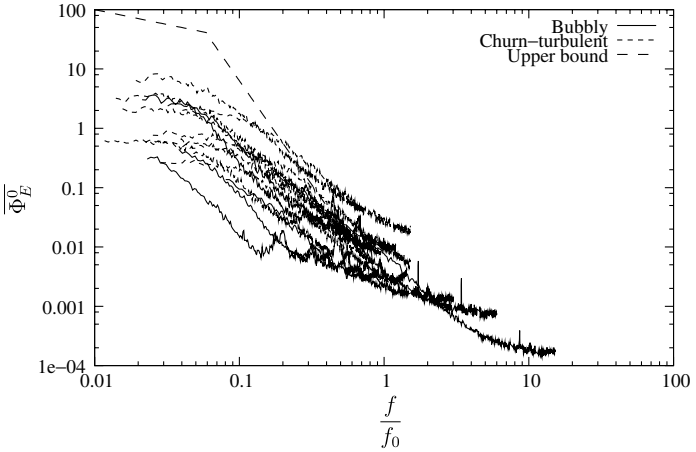

Fig. 15. Dimensionless reference equivalent spectra using Eq. (15).

the proposed upper bound, even when restricted to the same domain of reduced frequency (10^{-3}–1 Hz). But this comparison is limited by the fact that de Langre and Villard (1998) consider an homogeneous model for void fraction while we use local void fractions measured by bi-optical probe. The force scaling parameter is still based on gravity force, but the void length D_w is replaced by a length scale which considers the void fraction fluctuations. This new physical modelling enhances the efficiency in collapsing the present data. As a result, it gives a valuable insight into the two-phase underlying excitation mechanism.

4.3. Discussion

It would be appropriate to conclude this section with a clarification of some issues which merit closer examination. Firstly, it is worth mentioning that the presented results are partly depending on the choice of the experimental database and that the solutions proposed for the scaling factors are not unique. For instance, in case of a dispersed flow, the local interfacial area concentration can be expressed with the relation:

$$C_{a_I} = \frac{4N_b}{T}\frac{1}{V_g} = 4f_b\frac{1}{V_g} \tag{16}$$

This relation is based on a simple statistical approach found in Galaup (1975) and Veteau (1981), assuming spherical bubble and axial bubble velocity.

Since the local void fraction is related to the local interfacial area concentration by the relation:

$$\alpha = \frac{d_b}{6}C_{a_I} \tag{17}$$

it leads to the following expression for the bubble count rate:

$$f_b = \frac{3}{2}\frac{\alpha V_g}{d_b} \tag{18}$$

Except for two tests, Fig. 16 illustrates the very good agreement between the BOP direct measurement and the relation (18).

Additionally, for the force spectra, the cylinder diameter dependence is differently experienced according to the flow regime. For the bubbly regime, a D^2 dependence is observed while for the churn-turbulent regime the cylinder diameter dependence appears in D^3 as for single-phase dimensionless analysis (Axisa et al., 1990). This is due to the difference in the f_0 expression. Additional tests will be later performed with different cylinder diameters in order to study this dependence.

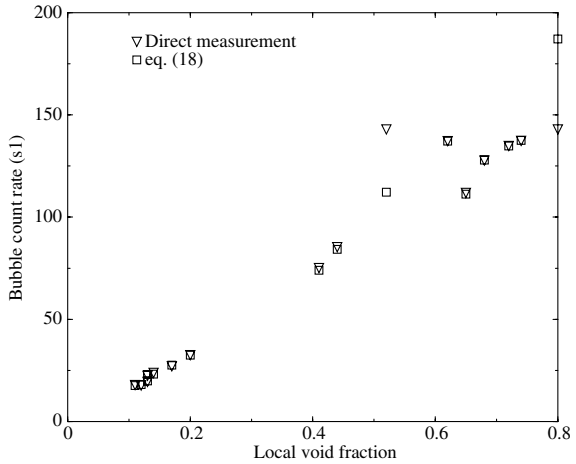

Fig. 16. Comparison between the bubble count rate measurement and Eq. (18) formulation.

5. Conclusion

We have presented a basic exploration to assess the buffeting lift forces exerted on a rigid cylinder in air–water cross-flow. A limited number of new experimental data has led to tackle the problem using a reduced dimensional analysis. In particular, this method helps indicating which parameters should preferably be first measured during present and future experiments. The central results of the paper are summarized as follows:

- A new experimental dataset – AMOVI 2005 – is available, which characterizes air–water vertical flows crossed by a rigid cylinder, with void fractions ranging from 10% to 80%. The innovative aspect is the simultaneous measurement of local characteristics of two-phase flow by means of a bi-optical probe and buffeting lift forces on the cylinder by means of a force cell.
- On examination of pertinent scaling factors of the buffeting lift force spectra, we have revealed the role of the two-phase flow regime as well as of two primary local parameters, the void fraction fluctuations and the bubble count rate.
- Under bubbly flow, the proposed scaling relationship, based on local void fraction fluctuations and bubble count rate provides a very efficient collapse of dimensionless spectra in the frequency domain.
- For churn-turbulent regime (void fraction $\geqslant 41\%$), these experiments have shown a natural cluster of the force spectra. Fluctuation intensity seems to have reached a maximum before decreasing at higher void fractions.
- For the moment, this model has been validated only for the experiments which have enabled its development. In particular it should not be used "as is" for tube bundle geometries.

Finally, it should be stressed that the proposed model, developed from the measurements of the local flow characteristics, cannot be extended straightaway to the mean parameters which alone are generally available. Thus, complementary studies are still necessary to extend this model to industrial applications.

Acknowledgements

The authors would like to thank Ph. Piteau and Th. Valin from Saclay CEA research center, for performing the tests in AMOVI mock-up. This research was supported by EDF and AREVA NP, and their help is gratefully acknowledged.

References

Axisa, F., Antunes, J., Villard, B., 1990. Random excitation of heat exchanger tubes by cross-flows. J. Fluids Struct. 4, 321–341.

Axisa, F., Villard, B., 1992. Random excitation of heat exchanger tubes by two phase cross-flow. In: Proceedings of 4th International Symposium on Flow-Induced Vibration and Noise, vol. 1. ASME, New York, pp. 119–139.

Blevins, R., 1991. Flow-induced vibration, second ed. Van Nostrand Reinhold, New York, ISBN 1-57524-050-5.

Cheng, H., Hills, J., Azzorpardi, B., 1998. A study of the bubble-to-slug transition in vertical gas–liquid flow in columns of different diameters. Int. J. Multiphase Flow 24, 431–452.

Cheung, J., Melbourne, W., 1983. Turbulence effects on some aerodynamic parameters of a circular cylinder at supercritical Reynolds numbers. J. Wind Eng. Indust. Aerodynam. 14, 399–410.

de Langre, E., Villard, B., 1998. An upper bound on buffeting forces caused by two-phase flows across tubes. J. Fluids Struct. 12, 1005–1023.

de Langre, E., Beaufils, B., Antunes, J., 1991. The numerical prediction of vibrations in tube bundles induced by cross-flow turbulence. Proceedings of 5th International Symposium and Flow-induced Vibration. I. Mech. E., UK London, pp. 253–260.

Delhaye, J., Giot, M., Riethmuller, M., 1981. Thermo-hydraulics of Two-phase Systems for Industrial Design and Nuclear Engineering. McGraw Hill, ISBN 0-07-016268-9.

Endres, L., Moller, S., 2001. Looking for correct dimensionless parameters for tube-bank flow analysis. J. Fluids Struct. 15, 737–750.

Friberg, P., 1998. Three-dimensional modelling of gas/liquid flow processes in bioreactors. Ph.D. Thesis, Telemark College, Porsgrunn, Norway.

Galaup, J., 1975. Contribution à l'étude des méthodes de mesure en écoulement diphasique. Ph.D. Thesis, Université Scientifique et Médicale de Grenoble, INPG.

Grossetête, C., 1995. Caractérisation expérimentale et simulations de l'évolution d'un écoulement diphasique à bulles ascendant dans une conduite verticale. Ph.D. Thesis, Ecole Centrale, Paris.

Hara, F., 1982. Two-phase cross-flow-induced forces acting on a circular cylinder. Proceedings of Flow-Induced Vibration of Circular Cylindrical Structures. In: ASME PVP, vol. 63. Springer, pp. 9–17.

Hassan, Y., Schmidl, W., Ortiz-Villafuerte, J., 1998. Investigation of three-dimensional two-phase-flow structure in a bubbly pipe flow. Measur. Sci. Technol. 9, 309–326.

Inada, F., Nishihara, T., Morita, R., Sakashita, A., Mizutani, J., 2004. Flow-induced vibration of cross-shaped tube bundle (the stabilizing effect of circular tubes). Proceedings of Flow-Induced Vibration. Ecole Polytechnique, Paris, pp. 265–270.

Inoue, A., Kosawa, Y., Yokosawa, M., Aoki, S., 1986. Studies on two-phase cross flow – Part I : Flow characteristics around a cylinder. Int. J. Multiphase Flow 12, 149–167.

Ishii, M., Zuber, N., 1979. Drag coefficient and relative velocity in bubbly, droplet or particulate flows. AIChE J. 25, 843–855.

Le Gall, F., Pascal-Ribot, S., Leblond, J., 2001. NMR measurements of fluctuations in air–water two-phase flow: pipe flow with and without "disturbing" section. Phys. Fluids 13, 1118–1129.

Lian, H., Noghrehkar, G., Chan, A., Kawaji, M., 1997. Effect of void fraction on vibrational behavior of tubes in tube bundle under two-phase cross flow. J. Vib. Acoust. 119, 457–463.

Matuszkiewicz, A., Flamand, J., Bouré, J., 1987. Bubble-slug flow pattern transition and instabilities of void fraction waves. Int. J. Multiphase Flow 13, 199–217.

Mercadier, Y., 1981. Contribution à l'étude des propagations de perturbations de taux de vide dans les écoulements diphasiques eau-air à bulles. Ph.D. Thesis, Université scientifique et médicale Institut national polytechnique, Grenoble, France.

Mishima, K., Ishii, M., 1984. Flow regime transition criteria for upward two-phase flow in vertical tubes. Int. J. Heat Mass Transfer 27, 723–737.

Murai, Y., Sasaki, T., Ishikawa, M., Yamamoto, F., 2005. Bubble-driven convection around cylinders confined in a channel. J. Fluids Eng. 127, 117–123.

Nakamura, T., Fujita, K., Kawanishi, K., Yamaguchi, N., Tsuge, A., 1991. Study on the vibrational characteristics of a tube array caused by two-phase flow. Part 1: Random vibration. In: Proceedings of PVP Flow-Induced Vibration and Wear, vol. 206, pp. 19–24.

Oengoren, A., Ziada, S., 1995. Vortex shedding, acoustic resonance and turbulent buffeting in normal triangle tube arrays. In: Proceedings of 6th International Conference on Flow-Induced Vibration, London, pp. 295–313.

Pascal-Ribot, S., Blanchet, Y., 2005. Study of relation between local parameters of two-phase flow and random forces on a cylinder. In: Proceedings of 11th International Topical Meeting on Nuclear Thermal-Hydraulics, CD-ROM, #308.

Pettigrew, M., Taylor, C., Jong, J., Currie, I., 1994. Vibration of tubes bundles in two-phase freon cross-flow. ASME J. Flow-Induced Vib. 273, 211–219.

Serizawa, A., Huda, K., Yamada, Y., Kataoka, I., 1997. Experimental and numerical simulation of bubbly two-phase flow across horizontal and inclined rod bundles. Nucl. Eng. Des. 175, 131–146.

So, R., Savkar, S., 1981. Buffeting forces on rigid circular cylinders in cross flows. J. Fluid Mech. 105, 397–425.

Szirtes, T., 1997. Applied Dimensional Analysis and Modeling. McGraw-Hill, ISBN 0-07-062811.

Taitel, Y., Bornea, D., Dukler, A., 1980. Modelling flow pattern transitions for steady upward gas–liquid flow in vertical tubes. AIChE J. 26, 345–354.

Taylor, C., Pettigrew, M., 2001. Effect of flow regime and void fraction on tube bundle vibration. ASME J. Press. Vess. Technol. 123, 407–413.

Taylor, C., Currie, I., Pettigrew, M., Kim, B., 1989. Vibration of tube bundles in two-phase cross-flow: Part 3 – Turbulence induced excitation. ASME J. Press. Vess. Technol. 111, 488–500.

Taylor, C., Pettigrew, M., Currie, I., 1992. Random excitation forces in tube arrays subjected to two-phase cross-flow. In: Proceedings of ASME International Symposium on Flow-Induced Vibration and Noise, vol. 1. Anaheim, California, USA, pp. 89–107.

Taylor, C., Pettigrew, M., Currie, I., 1996. Random excitation forces in tube bundles subjected to two-phase cross-flow. ASME J. Press. Vess. Technol. 118, 265–277.

Veteau, J.-M., 1981. Contribution à l'étude des techniques de mesure de l'aire interfaciale dans les écoulements à bulles. Ph.D. Thesis, Université Scientifique et Médicale de Grenoble, INPG.